ELSEVIER

Applied Catalysis A: General 130 (1995) 195–212

APPLIED CATALYSIS A: GENERAL

# Oxidative coupling of methane in a mixed-conducting perovskite membrane reactor

J.E. ten Elshof *, H.J.M. Bouwmeester, H. Verweij

*University of Twente, Department of Chemical Technology, Laboratory of Inorganic Materials Science, P.O. Box 217, 7500 AE Enschede, Netherlands*

Received 1 March 1995; revised 19 April 1995; accepted 19 April 1995

**Abstract**

Ionic–electronic mixed-conducting perovskite-type oxide $La_{0.6}Sr_{0.4}Co_{0.8}Fe_{0.2}O_3$ was applied as a dense membrane for oxygen supply in a reactor for methane coupling. The oxygen permeation properties were studied in the $p_{O_2}$-range of $10^{-3}$–1 bar at 1073–1273 K, using helium as a sweeping gas at the permeate side of the membrane. The oxygen semi-permeability has a value close to 1 mmol $m^{-2}$ $s^{-1}$ at 1173 K with a corresponding activation energy of 130–140 kJ/mol. The oxygen flux is limited by a surface process at the permeate side of the membrane. It was found that the oxygen flux is only slightly enhanced if methane is admixed with helium. Methane is converted to ethane and ethene with selectivities up to 70%, albeit that conversions are low, typically 1–3% at 1073–1173 K. When oxygen was admixed with methane rather than supplied through the membrane, selectivities obtained were found to be in the range 30–35%. Segregation of strontium was found at both sides of the membrane, being seriously affected by the presence of an oxygen pressure gradient across it. The importance of a surface limited oxygen flux for application of perovskite membranes for methane coupling is emphasized.

*Keywords:* Perovskite; $La_{0.6}Sr_{0.4}Co_{0.8}Fe_{0.2}O_3$; Conductivity (mixed); Oxygen permeation; Methane coupling; Membrane reactor

## 1. Introduction

Many mixed oxides of the perovskite-type ($AMO_3$) show catalytic activity in oxidation reactions. The catalytic properties are closely related to the nature of the M-cation, as was shown for propane oxidation [1]. The A-site cation is in general catalytically inactive, but the partial substitution of the A-site cation by aliovalent ions has been used by several authors to control both the valency of the M-element

* Corresponding author. E-mail j.e.tenelshof@ct.utwente.nl, fax. (+31-53) 339546.


*SSDI* 0926-860X(95)00098-4

and the oxygen vacancy concentration in the bulk [2,3]. By this substitution the M–O bond strength and the mobility of the oxygen anions are affected. Since the oxygen ion conductivity is generally enhanced by the partial substitution of A-site cations by lower valent cations [4], oxygen ions in subsurface layers may be able to take part in the catalytic process. The intrafacial mechanism as suggested by Voorhoeve for oxidation reactions on perovskites [5] may be promoted by this, as it is generally believed that there is a connection between this mechanism and the ease of oxygen ion migration [6]. In addition to their high ionic conductivity some A-site substituted perovskite-type oxides with transition metal ions at the M-site show electronic conductivity [7]. As an example, the partial substitution of trivalent lanthanum in $LaMO_3$ (M is a transition metal cation) by divalent strontium, resulting in the solid solution $La_{1-x}Sr_xMO_3$, is given by

$$SrMO_3 \underset{LaMO_3}{\rightarrow} Sr_{La}' + M_M^{\cdot} + 3O_O^{x} \quad (1)$$

where the notation for defects is from Kröger and Vink [8]. Due to the above substitution the concentration of oxygen vacancies is promoted according to the defect reaction

$$2M_M^{\cdot} + O_O^{x} \rightleftharpoons 2M_M^{x} + V_O^{\cdot\cdot} + 1/2O_2(g). \quad (2)$$

Furthermore, M-site transition metal cations can show charge disproportionation:

$$2M_M^{x} \rightleftharpoons M_M^{\cdot} + M_M' \quad (3)$$

Ionic conduction can take place by hopping of oxygen ions to neighbouring vacant sites, whereas electronic conduction is thought to occur via $M^{n+}$–O–$M^{(n+1)+}$ conduction pairs [9].

Several perovskite-type oxides were already investigated as catalysts for the methane coupling reaction [10–15]. Some $LaCoO_3$-based perovskites, partially substituted with barium and iron on the A-and M-sites, respectively, were found to be active in the oxidative coupling reaction when the reaction was performed by the temperature-programmed reduction (TPR) method and cyclic operation [10]. A study of perovskites of the formula $Ca_{1-x}Sr_xTi_{1-y}M_yO_{3-\delta}$ (M = Fe or Co; $x = 0$–1; $y = 0$–0.6) indicated that these catalysts showing both ionic and p-type electronic conductivity give a high selectivity to the desired products [11]. A combined Mössbauer and catalytic study of $ACo_{0.8}Fe_{0.2}O_{3-\delta}$ (A = Ba, Sr, Ca) showed that the barium and strontium perovskites, which gave a high selectivity towards $C_2$ products ($C_2$ indicates the sum of ethane and ethene), have a disordered oxygen vacancy structure [12]. In contrast, the calcium-containing sample adopted the brownmillerite structure, which is known to have an ordered arrangement of oxygen vacancies. The performance of this composition was considerably less. Ca-doped $Ba_{0.95}Ca_{0.05}Co_yFe_{1-y}O_{3-\delta}$ ($y \geqslant 0.8$) showed even better catalytic properties in comparison with the above mentioned $BaCo_yFe_{1-y}O_{3-\delta}$ [13]. It was considered by the authors that the oxygen deficiency of $BaCo_yFe_{1-y}O_3$ was small and that it

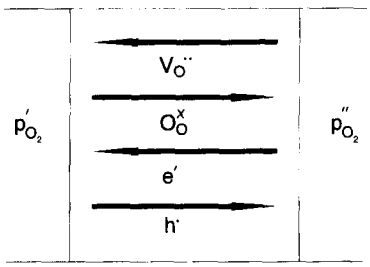


Fig. 1. Fluxes in mixed conducting membrane under the influence of a partial pressure gradient. $p_{O_2}'$ is higher oxygen partial pressure, $p_{O_2}''$ is lower oxygen partial pressure.

tended to contain mixed oxides of different structures. By doping a small amount of Ca the perovskite structure was stabilized and its nonstoichiometry increased, which was thought to contribute to the improved $C_2$ selectivity.

The simultaneous occurrence of ionic and electronic conductivity makes that these materials can be applied as oxygen semipermeable membranes in membrane reactors. Teraoka et al. were the first to measure steady-state oxygen permeation through mixed-conducting $La_{1-x}A_xCo_{1-y}M_yO_{3-\delta}$ membranes (A = Sr, Ca; M = Fe, Co, Cu, Ni) directly [16,17]. Higher oxygen fluxes were observed with increasing level of A-site substitution and reducibility of the perovskites [18]. Since these initial studies, compositions of $La_{1-x}Sr_xCo_{1-y}Fe_yO_{3-\delta}$ have been claimed in patents for use as oxygen separation membrane, e.g. for the production of oxygen [19].

The principle of a membrane, semipermeable to oxygen, is shown in Fig. 1. By applying an oxygen partial pressure gradient across the membrane, oxygen is driven from the high to the low partial pressure side. Local charge neutrality is maintained by the joint diffusion of oxygen vacancies and electrons or electron holes. The net flux is determined by the species with the smallest conductivity. Wagner's theory of oxide film growth [20,21] on metals is generally used to describe the oxygen flux across a membrane.

$$J_{O_2} = \frac{RT}{4^2F^2L}\int_{P_{O_2}''}^{P_{O_2}'} t_i t_{el}\sigma_{total}\,\mathrm{d}\ln p_{O_2} \tag{4}$$

Here $J_{O_2}$ is the oxygen permeation flux in mol $cm^{-2}$ $s^{-1}$, $t_i$ and $t_{el}$ are the ionic and electronic transference numbers, $\sigma_{total}$ ($=\sigma_{ion}+\sigma_{el}$) is the total conductivity ($\Omega^{-1}$ $cm^{-1}$), $p_{O_2}'$ and $p_{O_2}''$ are the oxygen partial pressures at the high and the low partial pressure side of the membrane, respectively; $L$ is the membrane thickness (cm). $R$, $F$ and $T$ refer to the gas constant (J $mol^{-1}$ $K^{-1}$), Faraday's constant (C $mol^{-1}$) and the temperature (K), respectively.

The oxygen permeability of $La_{0.6}Sr_{0.4}CoO_3$ was found to be roughly proportional to its ionic conductivity [22], which is in agreement with the fact that its electronic conductivity is several orders of magnitude larger. For several other $La_{1-x}Sr_xCo_{1-y}Fe_yO_{3-\delta}$ perovskites the electronic conductivity was also found to

control the total conductivity [4,23]. This implies that $t_{el} \approx 1$ so that the product $t_i t_{el} \sigma_{total}$ reduces to $\sigma_{ion}$ and the oxygen flux becomes proportional to the ionic conductivity. On the assumption that all oxygen vacancies are fully ionized, an expression for ionic conduction can be given on the basis of the Nernst–Einstein relation:

$$\sigma_{ion} = \frac{4F^2[V_O^{\cdot\cdot}]D_V}{RTV_m} \tag{5}$$

$[V_O^{\cdot\cdot}]$ is the oxygen vacancy mole fraction, $D_V$ the oxygen vacancy diffusion coefficient ($cm^2\ s^{-1}$) and $V_m$ the molar volume of the perovskite ($cm^3\ mol^{-1}$).

(Eq. 4) is valid only if the oxygen flux through the membrane is controlled by bulk diffusion through the oxide lattice. Reduction of the membrane thickness $L$ will in that case lead to higher oxygen fluxes. Teraoka mentioned the influence of sintering temperature on oxygen semipermeability [16], which may indicate that grain boundary diffusion plays a significant role. In addition, the oxygen flux may be influenced or limited by surface exchange kinetics [24]. A characteristic thickness $L_c$ has been identified, i.e. the membrane thickness at which the oxygen flux is equally determined by surface exchange kinetics and bulk transport. The value of $L_c$ can be calculated provided that the surface oxygen exchange rate and the oxygen diffusivity are known, e.g. from $^{18}O$–$^{16}O$ isotopic exchange techniques. In a previous paper [25] we reported on the use of $La_{1-x}Sr_xFeO_3$ membranes in the high temperature oxidation of carbon monoxide. It was shown that the oxygen permeation rate is limited by the reduction process at the surface in the lower partial pressure compartment.

From the above it is clear that mixed-conducting perovskite membranes may be used as oxygen supplying membrane and methane coupling catalyst at the same time. Otsuka was the first to use separated feeds of air and methane in a study in which oxygen was electrochemically pumped into the methane stream by using an yttria-stabilized zirconia (YSZ) electrolyte cell [26]. This approach has been attempted by several others and was reviewed recently [27]. It was shown that electrochemically pumped oxygen coupled more selectively than gaseous oxygen. Since the measured activation energies for $C_2$ and $CO_2$ formation differed when oxygen was supplied by electrochemical pumping rather than by premixing of molecular oxygen in the feed stream [28], it has been suggested that the active species is different in these two cases. Besides that lattice oxygen may couple methane more selectively than gaseous oxygen, air may be used as the oxidant instead of more expensive oxygen.

The observations that were made in the CO oxidation study on $La_{1-x}Sr_xFeO_3$ membranes [25] are of importance from a technological point of view, since they suggest that under actual operating conditions the depth of reduction of the oxide membrane surface can be kept limited. It implies that constraints regarding the structural integrity and chemical stability in reducing environments of potential membrane candidates can be relaxed. Therefore, $La_{0.6}Sr_{0.4}Co_{0.8}Fe_{0.2}O_{3-\delta}$ mem-

branes are used as oxygen separating membrane and methane coupling catalyst in the present study. Cobalt was partially substituted by Fe to increase the chemical stability of the perovskite in reducing atmospheres. The results are compared with those observed when the membrane is placed in a single-chamber reactor and oxygen is admixed with the methane feed stream.

## 2. Experimental

### 2.1. Membrane preparation

Nitrates of the constituent metals (Merck, p.a. quality) were separately dissolved in Q2-water and their concentrations were determined by titration with EDTA. Stoichiometric amounts of the solutions were taken and mixed. A solution of ammonia/EDTA was added to the mixed metal solution, the final concentration of EDTA being 1.5 times the total metal cation concentration. The pH of the solution was adjusted to 8–9 by using ammonia. The solution was mixed for several hours under moderate heating to complete complexation and then pyrolysed in a stove at 500 K. The resulting powder was milled for several hours in a planetary mill in acetone and after drying calcined at 1200 K in stagnant air for 12 h. Calcination at lower temperatures also resulted in perovskite formation but in these cases X-ray diffraction (XRD) revealed traces of $SrCO_3$. After repeating the milling procedure disks of 25 mm diameter were obtained by uniaxial pressing at 1.5 bar, followed by isostatic pressing at 4000 bar. The disks were sintered in Pt-lined boats at 1450–1500 K for 24 h in a pure oxygen atmosphere. Membranes of 15.2 mm diameter and 0.5–2 mm thickness were cut from the sintered disks. Prior to use the membranes were polished with 1000 MESH SiC and ultrasonically cleaned in ethanol. An Archimedes method was used to determine the density of the membranes.

### 2.2. Experimental set-up

Oxygen permeation measurements were performed in a quartz reactor [25] with a reactor volume of approximately 3 ml. Catalytic experiments were performed in a quartz reactor depicted in Fig. 2. Supremax glass rings (Schott Nederland B.V.) were used to seal the membrane into the quartz reactor at 1310–1330 K in stagnant air, thus creating two isolated chambers.

The experimental set-up is shown in Fig. 3. In the higher oxygen partial pressure compartment the oxygen partial pressure was monitored by an YSZ-based oxygen sensor. The oxygen partial pressure in this compartment could be adjusted in the range $10^{-2}$–1 bar by admixing $N_2$, air and $O_2$. The total flow rate in this compartment was kept high [100–180 ml/min (STP)] to prevent mass transfer limitations from the gas phase. Brooks 5800 mass flow controllers were used to control the gas flow rates through both compartments. A Varian 3300 gas chromatograph and

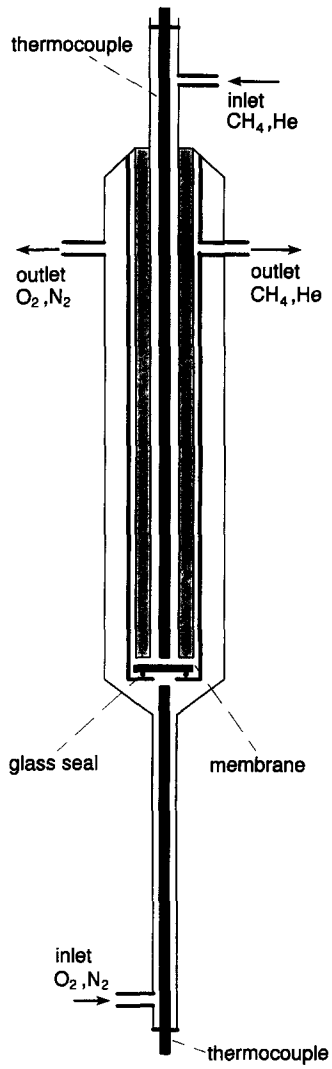


Fig. 2. Schematic diagram of the catalytic reactor.

a LDC/Milton Roy CL-10 integrator were used for analysis of the compositions at both the inlet and outlet of the lower oxygen partial pressure compartment of the reactor. A molecular sieve 13X was used for separation of $H_2$, $O_2$, $N_2$, $CH_4$ and CO. A Porapak-N column was used for separation of $CO_2$, hydrocarbons and $H_2O$. The total gas flows at the inlet and outlet of the reactor were separately measured by a Brooks Volumeter.

### *2.3. Permeation and catalytic measurements*

In the oxygen permeation measurements the oxygen partial pressure at the lean side of the membrane was varied by adjusting the He (4.6 N) flow rate in the range

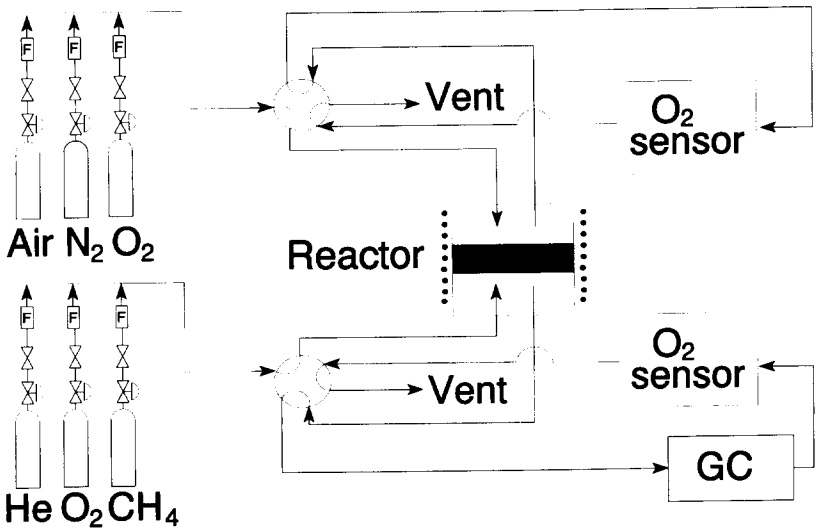


Fig. 3. Schematic diagram of the experimental set-up.

5–70 ml/min (STP). The gas tightness of membrane and seal was checked by GC detection of nitrogen in the effluent stream, since in case of a leak free membrane no $N_2$ will be present there. The contribution of leakage to the total oxygen flux could be calculated from the measured nitrogen concentration and was found to be less than 3% in all cases, and typically well below 1%. Calculated oxygen permeation fluxes were corrected for this contribution.

In the catalytic measurements the feed consisted of He and $CH_4$. The permeation was calculated from the outlet flow rate and the concentrations of all oxygen containing species ($O_2$, CO, $CO_2$ and $H_2O$). Selectivities were calculated from the total amounts of products formed. The carbon balance was in all cases in the range $99 \pm 2\%$. Oxygen fluxes and reaction rates were normalized with respect to the geometric surface area exposed to the methane/helium atmosphere.

To compare the results with the effect of cofed oxygen, measurements were also performed in a single-chamber reactor with similar geometry and dimensions. An amount of oxygen was admixed with methane which was equal to the amount of permeated oxygen measured under similar conditions. These experiments will be referred to as 'cofeed mode', as distinct from the 'membrane mode' described above.

### 2.4. XRD, SEM, EDX and AES

Sample characterisation was performed by taking XRD spectra (Philips PW1710) from crushed sintered membranes using Ni-filtered Cu $K\alpha_1$ (1.5406 Å) radiation. $LaB_6$ was added as an internal standard and the samples were measured with a $2\theta$ scan from 20° to 140° with steps of 0.018°. The intensity was collected during 5–10 s.

The membrane surface morphology was examined by high resolution scanning electron microscopy (HR-SEM) (Hitachi S-800 field emission microscope). Phases present at the surface were determined by XRD. Surface element analysis was performed by energy dispersive X-ray (EDX) (Kevex Delta Range) and by analytical electron spectroscopy (AES) (Perkin Elmer PHI 600). An Auger depth profile was obtained by sputtering with a 1 $mm^2$ 3.5 keV $Ar^+$ beam on 30° tilted samples with a sputter rate of 32.5 Å $min^{-1}$ ($\pm$ 10%). The incident angle between the beam and the sample was 45° and the surface area analyzed was $150 \times 120$ $\mu m^2$.

## 3. Results and discussion

### 3.1. XRD

The XRD spectra of powders obtained from crushed freshly prepared membranes showed a single-phase perovskite. All peaks could be indexed on the basis of a rhombohedrally distorted cubic cell with lattice parameters $a = 5.4450(9)$ Å and $c = 13.2553(3)$ Å (hexagonal setting), in close agreement with crystallographic data on $La_{0.6}Sr_{0.4}CoO_3$ [29]. On the basis of the unit cell volume, the densities of membranes used in this study were calculated to be in the range of 96.5–98.0% of theoretical.

### 3.2. Oxygen permeation measurements

The Arrhenius curves of the oxygen flux in an air/He gradient are shown in Fig. 4 for two samples of different thickness. After sealing the samples were cooled down to temperatures between 1223–1273 K and kept at this temperature until the permeation became stable (10–15 h). At the He side an oxygen partial pressure of 0.017 bar was maintained. As can be seen from the figure the two curves coincide well in absolute magnitude.

In contrast, the stabilization times of membranes which were immediately cooled down from the temperature at which sealing was performed to 1100–1200 K were considerably longer and their final permeability was a factor of 3–4 lower than is

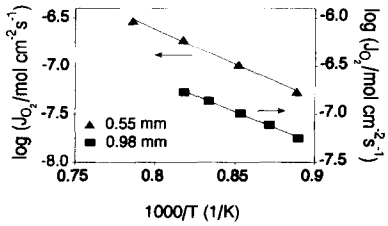


Fig. 4. Temperature dependence of oxygen permeation flux in air/He (0.017 bar $O_2$) gradient for samples of different thicknesses.

Table 1
Activation energies of oxygen semi-permeability of $La_{0.6}Sr_{0.4}Co_{0.8}Fe_{0.2}O_3$ in an air/He gradient

| Thickness (mm) | $T$ (K) | $E_{act}$ (kJ/mol) |
|---|---|---|
| 0.55 | 1123–1273 | 138 ± 10 |
| 0.98 | 1123–1223 | 128 ± 8 |

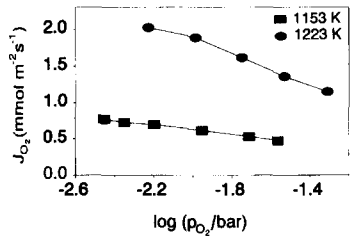


Fig. 5. Dependence of oxygen flux on partial pressure in lower partial pressure compartment at different temperatures.

expected on the basis of the results shown in Fig. 4. Upon increasing the temperature to 1200–1300 K, the fluxes through these membranes increased irreversibly and their performances became similar to those of the high-temperature stabilized samples.

The activation energies obtained from the Arrhenius plots in Fig. 4 are given in Table 1. Itoh et al. calculated an activation energy of 117 kJ/mol for the ionic conductivity from oxygen permeation data of $La_{0.6}Sr_{0.4}CoO_3$ [30]. The authors used a simple logarithmic dependence for the oxygen flux, which can be derived from (Eq. 4) assuming a constant ionic conductivity. It is plausible that the activation energy for $La_{0.6}Sr_{0.4}Co_{0.8}Fe_{0.2}O_3$ is slightly higher due to the presence of iron.

Fig. 5 shows the oxygen permeation flux in an air/He gradient as a function of the oxygen partial pressure in the lower partial pressure compartment. The measurements were performed on two different samples of 1.0 mm thickness at different temperatures. Stabilization was performed at the temperature of measurement. The difference in permeation rates correspond well with the observed activation energy. A strong indication for a surface controlled flux emerges from the dependence of the oxygen flux on the partial pressure. For all membranes measured, the oxygen flux can be related to the oxygen partial pressure in the He-containing chamber via

$$J_{O_2} \propto p_{O_2}^{n} \tag{6}$$

where $n = 0.22 \pm 0.01$. When a mass action type relation is applied to (Eq. 2), taking into account that the oxygen stoichiometry is defined by $[O_O^x] = 3 - [V_O^{\cdot\cdot}]$, the following relation holds for the oxygen vacancy concentration:

$$[V_O^{\cdot\cdot}] = \frac{3[M_M^{\cdot}]^2}{[M_M^{\cdot}]^2 + K_2[M_M^x]^2 p_{O_2}^{1/2}} \tag{7}$$

where $K_2$ is the equilibrium constant. The power dependence of the oxygen vacancy concentration on oxygen partial pressure will thus vary between $-1/2$ and 0, depending on oxygen partial pressure and temperature. From Eqs. (4), (5) and (7) the same power dependence is expected for the oxygen flux. A positive $n$-value as is experimentally found here may indicate that a process other than bulk diffusion limits the oxygen flux. Combined with the data presented in Fig. 4, as discussed above, we take this as evidence of a surface-exchange controlled flux.

Measurements at 1153 K were performed in which the partial pressure in the higher partial pressure compartment was varied (0.01–0.21 bar), while the oxygen concentration at the He side was kept at a constant value of 5200 ppm. In these cases the value of $n$ is close to zero. The experimental oxygen fluxes can be represented by

$$J_{O_2}(\text{mmol m}^{-2}\,\text{s}^{-1}) = 1.054 + 0.506 \log p_{O_2}' \tag{8}$$

It has been shown [31] that the $p_{O_2}$ dependency is strongly dependent on the applied gradient. This also becomes clear when (Eq. 7) is considered. The oxygen vacancy concentration will be different on both sides of the membrane. Thus, the differences in dependencies as found here do not necessarily indicate a difference in the nature of the rate-determining step of the permeation process.

### 3.3. Catalytic measurements

The temperature dependence of the catalytic activity and $C_2$ selectivity was determined by feeding 0.25 bar methane at a total flow of 16.4 ml/min (STP) (2.79 $\mu$mol $s^{-1}$ $CH_4$). Air was supplied at the high oxygen partial pressure side of the membrane. The results are shown in Fig. 6. After an initial increase of the selectivity between 1073 and 1123 K to 62%, a slight decrease is observed between 1123 and 1173 K, followed by a steep decrease above 1173 K to finally reach 41% at 1223 K. The selectivity drop can be attributed to a strong increase of the production rate of $CO_2$. Since this rate increase is accompanied by a strong increase of the $H_2$ production rate it is likely that above 1173 K carbon deposition occurs by thermal decomposition of methane, followed by oxidation with unreacted permeated oxygen. The activation energy for oxygen permeation was determined to be $169 \pm 6$ kJ/mol. Although this value is about 35 kJ/mol higher than determined

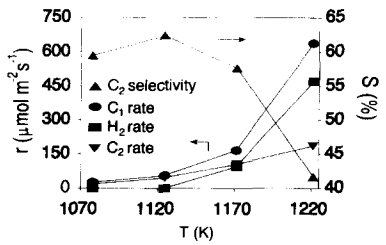


Fig. 6. Reaction rates and selectivity to ethane/ethene as function of temperature. $p_{CH_4} = 0.25$ bar. Total flow rate is 16.4 ml/min (STP).

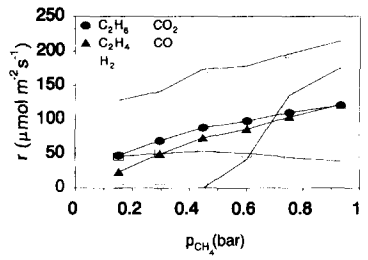


Fig. 7. Reaction rates at 1153 K as function of the methane partial pressure at a total flow rate of 20.5 ml/min (STP).

from air/He measurements, the difference is likely to be due to the fact that stabilization was performed at 1073 K only.

The activation energy for methane conversion was $217 \pm 12$ kJ/mol, while that of $C_2$ formation was calculated to be $175 \pm 10$ kJ/mol. In the aforementioned temperature range, the $C_2$ yield varied between 0.25% and 3.1%. From these results 1153 K was selected as standard temperature for further experiments, since both reasonable selectivities and oxygen fluxes are found here.

The methane partial pressure dependence at a total flow rate of 20.5 ml/min (STP) is shown in Fig. 7. Air was again supplied in the high partial pressure chamber. The oxygen flux was found to be $0.84 \pm 0.05$ mmol $m^{-2}$ $s^{-1}$ and was not influenced by changing the methane partial pressure. At methane pressures above 0.5 bar production of $H_2$ is seen, probably due to thermal decomposition of methane. The rate of carbon monoxide formation was virtually independent of the methane partial pressure, while the rates of formation of ethane, ethene and carbon dioxide steadily increased. The methane conversion ranges between 2.6 and 1.1%, to be compared with 0.45–0.35% from blank experiments.

Methane conversion, selectivities and relative oxygen consumption are given in Table 2. The oxygen consumption $X_{O_2}$ (defined as the total amount of oxygen consumed by reaction divided by the total amount of oxygen permeated) increases from 44% to 75% upon increasing the methane partial pressure from 0.15 bar to 0.93 bar. Thus, gaseous oxygen is observed in the methane containing compartment, and $p_{O_2}$ varies there between $10^{-2.21}$ and $10^{-2.55}$ bar. Comparing the observed oxygen flux with the results shown in Fig. 5 clarifies that the oxygen flux is not or only slightly enhanced by the presence of methane.

Table 2
Methane conversion, selectivities and relative oxygen consumption as a function of $p_{CH_4}$. $T = 1153$ K; flow rate is 20.5 ml/min (STP)

| $p_{CH_4}$ (bar) | $X_{CH_4}$ (%) | $S_{CO}$ (%) | $S_{CO_2}$ (%) | $S_{C_2H_4}$ (%) | $S_{C_2H_6}$ (%) | $X_{O_2}$ (%) |
|---|---|---|---|---|---|---|
| 0.15 | 2.6 | 14.5 | 40.5 | 14.8 | 30.1 | 43.8 |
| 0.30 | 1.9 | 11.6 | 32.3 | 22.8 | 31.6 | 49.9 |
| 0.60 | 1.3 | 8.3 | 29.1 | 28.0 | 31.9 | 66.6 |
| 0.93 | 1.1 | 5.0 | 27.8 | 31.4 | 31.2 | 74.7 |

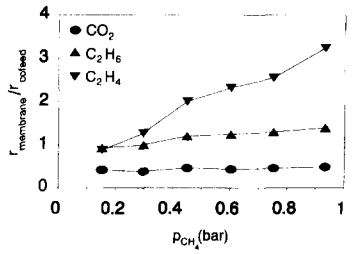


Fig. 8. Ratios of reaction rates in membrane mode and cofeed mode at 1153 K as function of methane partial pressure. Flow rate is 20.5 ml/min (STP).

Fig. 8 shows the ratios of the production rates of $C_2$ products and $CO_2$ as a function of $p_{CH_4}$ when operating in the membrane mode and cofeed mode. No production of carbon monoxide was observed in the cofeed mode. It is seen that the selectivity to ethane/ethene is much higher in the membrane mode. Not only the production rate of carbon dioxide is 40–50% of that in the cofeed mode, the rates of ethane and ethene formation are considerably higher. At $p_{CH_4} = 0.93$ bar, the rates of ethane and ethene formation equal 1.4 and 3.2 times those in the cofeed mode, respectively. The production rates obtained using membrane and cofeed mode, as well as those from blank experiments (without catalyst), are given in Table 3. The presence of the catalyst leads to a large increase in the production rate of $CO_2$. At low methane partial pressures the production rates of ethane and ethene are substantially higher in cofeed mode than in the blank experiments, but at 0.93 bar this difference is almost negligible. Although the rate of $CO_2$ production is also high in membrane mode, the rate of $C_2$ production becomes higher than in the other two cases for high $p_{CH_4}$.

To compare the $C_2$ selectivity as a function of the methane conversion in both modes of operation, methane was fed to the reactor with a partial pressure of 0.40 bar, while the conversion was varied by changing the total flow rate. The results are shown in Fig. 9. The selectivity of the membrane process is considerably higher than that of the cofeed process. These results may indicate that the nature of the catalyst is different in the two cases. However, due to the high temperatures applied in these experiments, the role of the gas phase reactions can not be underestimated. Therefore, the results may also be attributed to a simple mass transport effect. Since the concentration profile of oxygen throughout the reactor will be different in the

Table 3
Production rates at different methane partial pressures in membrane mode and cofeed mode. 'Blank' refers to cofeed mode measurements with polished quartz membrane. Flow is 20.5 ml/min (STP)

| $p_{CH_4}$ (bar) | $CO_2$ ($\mu$mol $m^{-2}$ $s^{-1}$) | | | $C_2H_6$ ($\mu$mol $m^{-2}$ $s^{-1}$) | | | $C_2H_4$ ($\mu$mol $m^{-2}$ $s^{-1}$) | | |
|---|---|---|---|---|---|---|---|---|---|
| | Membrane | Cofeed | Blank | Membrane | Cofeed | Blank | Membrane | Cofeed | Blank |
| 0.15 | 128 | 305 | 8 | 48 | 51 | 19 | 23 | 27 | 0 |
| 0.45 | 174 | 370 | 12 | 88 | 73 | 44 | 73 | 36 | 16 |
| 0.93 | 215 | 437 | 17 | 121 | 86 | 77 | 122 | 37 | 38 |

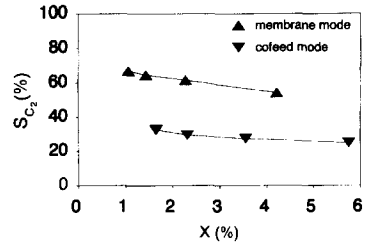


Fig. 9. $C_2$ selectivities versus methane conversion at 1153 K for membrane mode and cofeed mode. $p_{CH_4}$ at inlet is 0.40 bar.

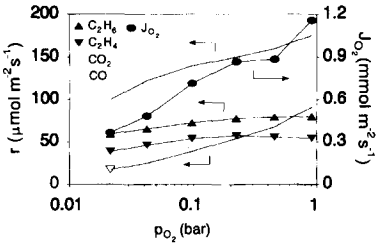


Fig. 10. Reaction rates and oxygen flux at 1153 K as function of oxygen partial pressure in the oxygen-supplying compartment. Flow rate is 20.5 ml/min (STP). $p_{CH_4}=0.40$ bar.

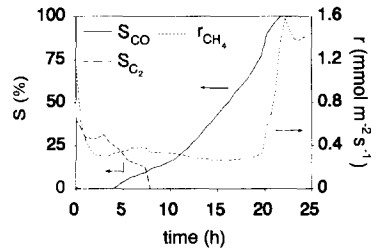


Fig. 11. Selectivities to $C_2$ and CO and conversion rate of methane at 1153 K as function of time in reduction experiment. Flow rate is 20.5 ml/min (STP). $p_{CH_4}=0.15$ bar.

two modes of operation, it could be suggested that the difference in selectivity results from a different $CH_4/O_2$ ratio in the vicinity of the surface. In the membrane mode the concentration of methane may be very low close to the surface, due to the continuous feeding of molecular oxygen from the surface, whereas in the cofeed mode, it would remain high.

The dependence of the oxygen partial pressure in the oxygen supplying compartment on the oxygen flux and reaction rates in the lower partial pressure chamber, when operating in membrane mode, is shown in Fig. 10. Roughly, a linear relation between $J_{O_2}$ and log $p_{O_2}$ is seen, in agreement with the results obtained from the permeation experiments. Increasing the oxygen partial pressure in the high partial pressure chamber mainly contributes to the conversion of methane to CO and $CO_2$. The rate of $C_2$ formation remains nearly constant.

The importance of a surface-exchange limited oxygen flux can be illustrated by an experiment in which a membrane was first equilibrated at 1153 K in a 1% $O_2$/He atmosphere and subsequently reduced in 15% $CH_4$/He (20 ml/min (STP); 2.0

$\mu$mol $s^{-1}$ $CH_4$). The experiment was performed in a single-chamber reactor as used in the cofeed mode experiments, but with no additional oxygen supplied after equilibration. The results are shown in Fig. 11. Initially, a $C_2$ selectivity of over 30% and a high methane conversion rate are reached. In the course of the experiment, the production of $C_2$ stops. CO production is seen after 4 h, accompanied by formation of hydrogen (not shown in the figure). After 20 h the selectivities to carbon monoxide and $H_2$ reach 100% and 93%, respectively. At the same time the methane conversion rate increases steeply. These results indicate that reduction of the perovskite to either basic oxides or metallic Co and/or Fe leads to an active catalyst for syngas production. Thus, in case of a bulk diffusion controlled oxygen flux the surface would become reduced by methane, until the membrane thickness has decreased to such an extent that the increase of the oxygen flux, due to the decreased membrane thickness, counterbalances the consumption of oxygen by methane.

The catalytic permeation experiments that were described in this paper were performed on samples that showed no deactivation, even after several weeks of continuous operation under varying conditions. Taking the results of the reduction experiment described above into account, this confirms that a surface exchange process limits the oxygen permeation process. Moreover, the reduction experiment shows that it may be possible to fine-tune the catalytic properties of the membrane by treatment of the membrane surface in a reducing atmosphere [32] or by adjustment of the amount of oxygen that is fed to the catalyst surface, either by cofeeding or by permeation.

### *3.4. Strontium segregation*

EDX analysis of samples after treatment in an air/He and/or air/He,$CH_4$ gradient showed an enrichment in Sr at both high and low partial pressure sides of the membrane. XRD analysis of the sample surfaces indicated the presence of $SrCO_3$ and $SrSO_4$. The origin of sulphur is not immediately clear, but it may be noted that the catalytic activity of $SrSO_4$ is known to be small [33]. To investigate the segregation in more detail, two samples were treated for 48 h at 1153 K in 0.25 bar $CH_4$ at a total flow of 20.5 ml/min (STP) and rapidly cooled down to room temperature. One sample was obtained after operation in the membrane mode, the other after operation in the cofeed mode under comparable conditions. Fig. 12 shows depth profiles made by Auger analysis on the membrane sides that had been exposed to methane. The profiles of Fe and Co are not shown in this figure, but their behaviour is similar to that as observed for La. Surface enrichment of Sr occurs in both cases. The segregation depth is about 15–30 nm for the sample obtained from the cofeed mode, while it extends over 60–80 nm in that from the membrane mode. This shows that not only segregation occurs in both modes of operation, but also that segregation might be affected by the presence of an oxygen potential gradient across the material, as occurs during operation in the membrane mode.

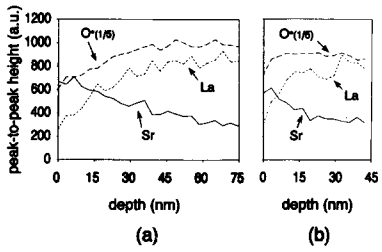


Fig. 12. Auger depth profiles of samples after 48 h treatment at 1153 K. $p_{CH_4} = 0.25$ bar. (a) Membrane mode, $p_{O_2}^{high} = 0.21$ bar. (b) Cofeed mode, $p_{O_2} = 0.01$ bar at inlet.

The influence of the oxygen partial pressure gradient on segregation can possibly be described in terms of kinetic demixing [34], but the precise mechanism is unclear.

A SEM picture of a cross-section of a sample exposed over 200 h to $CH_4$(He) at 1153 K after various catalytic experiments in the membrane mode is shown in Fig. 13. As can be seen the perovskite structure is preserved. However, the presence of molecular oxygen is required. In experiments where $O_2$ was absent, thermal decomposition of methane occurred easily. At the temperatures used here, Sr reacts with the deposited carbon to form $SrCO_3$. This reaction probably enhances further

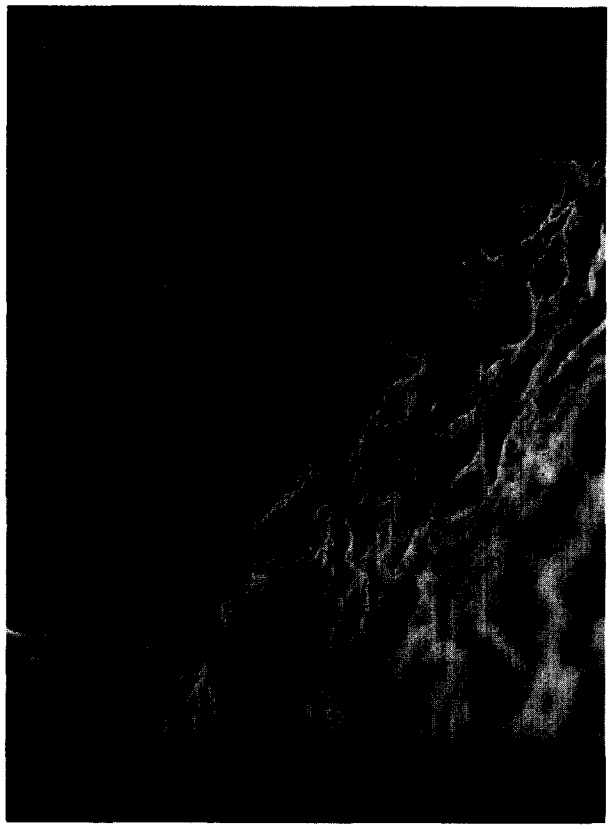

Fig. 13. SEM photograph of cross-section of membrane after treatment at 1153 K under varying conditions.

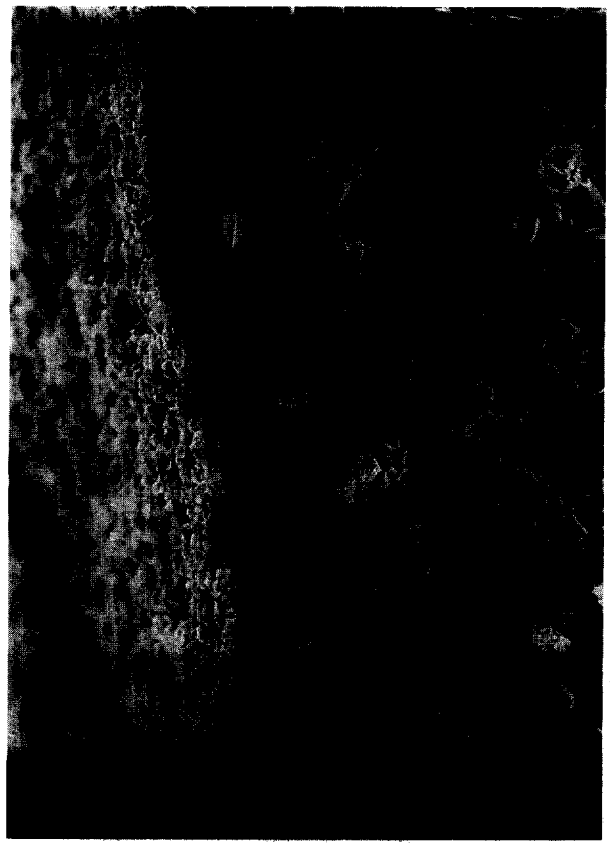

Fig. 14. SEM photograph of cross-section of membrane after treatment at 1100 K in air/1 bar $CH_4$ gradient for 3 days.

segregation of Sr. A SEM picture of a sample, treated for 3 days in pure $CH_4$ under permeation conditions at 1100 K, is shown in Fig. 14. At this temperature $SrCO_3$ is stable even in a $CO_2$-free atmosphere [35]. At the surface exposed to the ambient, a thin, highly porous $SrCO_3$ layer is present. Below this layer a porous, decomposed layer of about 10 $\mu$m, consisting mostly of La, Co and Fe is found. At a depth of about 10 $\mu$m, the bulk structure appears. Furthermore, the observation that this sample showed a much higher flux than expected on the basis of the results shown in this paper, suggests that the permeation flux increases with increasing surface area at the methane side.

## 4. Conclusions

Dense $La_{0.6}Sr_{0.4}Co_{0.8}Fe_{0.2}O_3$ membranes, free of microcracks, were prepared by making powders by thermal decomposition of metal nitrate solutions and subsequent sintering of the pressed powders. The densities were 96.5–98.0% of the

theoretical values. Permeation fluxes are typically 1 mmol $m^{-2} s^{-1}$ at 1173 K with an activation energy in the range of 130–140 kJ/mol. Since the oxygen flux remained constant with decreasing membrane thickness and increased with increasing surface area at the He-side of the membrane, it is concluded that the oxygen flux is limited by the release of oxygen at the He side of the membrane.

When the membrane was applied as an oxygen supplier and methane coupling catalyst, no enhancement of the oxygen flux could be observed in comparison with the fluxes observed in air/He gradients. For methane coupling purposes it is important that the oxygen flux is limited by surface exchange kinetics, since a bulk diffusion controlled flux would lead to reduction of the membrane surface, lowering the overall selectivity towards $C_2$ products.

At temperatures above 1170 K, substantial production of hydrogen was seen, which is likely due to thermal decomposition of methane. The $C_2$ selectivity decreased strongly above this temperature. At 1153 K, $C_2$ selectivities increased with increasing methane partial pressure, up to 67% at $p_{CH_4} = 0.93$ bar. Increasing the oxygen partial pressure in the oxygen supplying chamber was shown to contribute mainly to the formation of CO and $CO_2$.

When molecular oxygen was cofed with methane rather than supplied via the membrane, the $C_2$ selectivities were considerably lower (25–35%), due to a increased rate of $CO_2$ formation and lower rates of ethane and ethene formation. This may indicate that the nature of the catalyst is different in the membrane mode and cofeed mode of operation, possibly due to the presence of different types of active oxygen species at the surface. Segregation of Sr was found by EDX and AES. The depth of segregation is a factor of 2–3 larger in the membrane mode.

Substantial improvements of the methane conversion and selectivity may be expected from surface modification, e.g. the application of thin porous layers of well-known methane coupling catalysts such as Li/MgO or $Sr/La_2O_3$. The total supply of oxygen to the methane stream may be increased by enlargement of the surface area of the membrane. For industrial applications, the use of ceramic tubes instead of planar membranes will be advantageous, since large active surface areas per unit volume can be achieved in such geometries. Hazbun [36] proposed several multi-tube configurations, both with cross-flows and counter-flows of the methane and air streams.

## Acknowledgements

The support of the Commission of the European Communities in the framework of the Joule programme, sub-programme Energy from Fossil Resources, Hydrocarbons, is gratefully acknowledged. The authors would like to thank G. Mollenhorst and R. van den Blink for their help in the design and fabrication of the catalytic reactor.

## References

[1] T. Nitadori, T. Ichiki and M. Misono, Bull. Chem. Soc. Jpn., 61 (1988) 621.
[2] T. Nakamura, M. Misono and Y. Yoneda, J. Catal., 83 (1983) 151.
[3] T. Nitadori and M. Misono, J. Catal., 93 (1985) 459.
[4] S. Sekido, H. Tachibana, Y. Yamamura and T. Kambara, Solid State Ionics, 37 (1990) 253.
[5] R.J.H. Voorhoeve, J.P. Remeika and L.E. Trimble, Ann. N.Y. Acad. Sci., 3 (1976) 3.
[6] N. Yamazoe and Y. Teraoka, Catal. Today, 8 (1990) 175.
[7] W.L. Worrell, Solid State Ionics, 52 (1992) 147.
[8] F.A. Kröger, The Chemistry of Imperfect Crystals, North-Holland, Amsterdam, 1964.
[9] R.J.H. Voorhoeve, in J.J. Burton and R.L. Garten (Editors), Advanced Materials in Catalysis, Academic Press, New York, 1977, p. 129.
[10] T. Hayakawa, H. Orita, M. Shimizu, K. Takehira, A.G. Andersen, K. Nomura and Y. Ujihira, Catal. Lett., 16 (1992) 359.
[11] A.G. Andersen, T. Hayakawa, M. Shimizu, K. Suzuki and K. Takehira, Catal. Lett., 23 (1994) 59.
[12] K. Nomura, T. Goda, Y. Ujihira, T. Hayakawa and K. Takehira, Hyperfine Interactions, 69 (1991) 835.
[13] K. Nomura, T. Hayakawa, K. Takehira and Y. Ujihira, Appl. Catal. A, 101 (1993) 63.
[14] K. Omata, O. Yamazaki, K. Tomita and K. Fujimoto, J. Chem. Soc., Chem. Commun., (1994) 1647.
[15] D. Dissanayake, K.C.C. Kharas, J.H. Lunsford and M.P. Rosynek, J. Catal., 139 (1993) 652.
[16] Y. Teraoka, T. Nobunaga and N. Yamazoe, Chem. Lett., (1988) 503.
[17] Y. Teraoka, T. Nobunaga, N. Miura and N. Yamazoe, Solid State Ionics, 48 (1991) 207.
[18] T. Nakamura, G. Petzow and L.J. Gauckler, Mater. Res. Bull., 14 (1979) 649.
[19] R.M. Thorogood, R. Srinivasan, T.F. Yee and M.P. Drake, US Patent 5 240 480 (1993).
[20] C. Wagner, Z. Phys. Chem., 21 (1933) 25.
[21] M.H.R. Lankhorst, H.J.M. Bouwmeester and H. Verweij, Proc. 4th Intl. Conf. on Electronic Ceramics and Applications, 5–7 Sept. 1994, Aachen, Germany.
[22] Y. Teraoka, H.-M. Zhang, K. Okamoto and N. Yamazoe, Mater. Res. Bull., 23 (1988) 51.
[23] T. Inoue, J. Kamimae, M. Ueda, K. Eguchi and H. Arai, J. Mater. Chem., 3 (1993) 751.
[24] H.J.M. Bouwmeester, H. Kruidhof and A.J. Burggraaf, Solid State Ionics, 72 (1994) 185.
[25] B.A. van Hassel, J.E. ten Elshof and H.J.M. Bouwmeester, Appl. Catal. A, 119 (1994) 279.
[26] K. Otsuka, S. Yokoyama and A. Morikawa, Chem. Lett., (1985) 319.
[27] D. Eng and M. Stoukides, Catal. Rev.-Sci. Eng., 33 (1991) 375.
[28] H. Nagamoto, K. Hayashi and H. Inoue, J. Catal., 126 (1990) 671.
[29] Powder Diffraction File, JCPDS-International Centre for Diffraction Data, no. 36-1393.
[30] N. Itoh, T. Kato, K. Uchida and K. Haraya, J. Membrane Sci., 92 (1994) 239.
[31] J.E. ten Elshof, H.J.M. Bouwmeester and H. Verweij, Solid State Ionics, submitted for publication.
[32] J.O. Petunchi and E.A. Lombardero, Catal. Today, 8 (1990) 201.
[33] A.M. Maitra, I. Campbell and R.J. Tyler, Appl. Catal. A, 85 (1992) 27.
[34] H. Schmalzried, Solid State Reactions, Verlag Chemie, Weinheim, 1981.
[35] M.J. Scholten, J. Schoonman, J.C. van Miltenburg and H.A.J. Oonk, Solid State Ionics, 61 (1993) 83.
[36] E.A. Hazbun, US Patent 4 791 079 (1988).